# Quantifying immediate carbon emissions from El Niño-mediated wildfires in humid tropical forests

Kieran Withey[1], Erika Berenguer[1,2], Alessandro Ferraz Palmeira[3], Fernando D. B. Espírito-Santo[4], Gareth D. Lennox[1], Camila V. J. Silva[1], Luiz E. O. C. Aragão[5,6], Joice Ferreira[7], Filipe França[1,7,8], Yadvinder Malhi[2], Liana Chesini Rossi[9] and Jos Barlow[1]

[1]Lancaster Environment Centre, Lancaster University, Lancaster LA1 4YQ, UK
[2]Environmental Change Institute, University of Oxford, Oxford OX1 3QY, UK
[3]Instituto de Ciências Biológicas, Universidade Federal do Pará, Rua Augusto Corrêa, 01, Campus Guamá, Belém, PA CEP: 66075-110, Brazil
[4]Centre for Landscape and Climate Research (CLCR) and Leicester Institute of Space and Earth Observation (LISEO), School of Geography, Geology and Environment, University of Leicester, University Road, Leicester LE1 7RH, UK
[5]Remote Sensing Division, National Institute for Space Research, Avenida dos Astronautas, 1.758, 12227-010 São José dos Campos, São Paulo, Brazil
[6]College of Life and Environmental Sciences, University of Exeter, Exeter EX4 4RJ, UK
[7]Embrapa Amazônia Oriental, Travessa Dr Enéas Pinheiro, s/n, CP 48, 66095-100 Belém, Pará, Brazil
[8]Instituto Federal de Minas Gerais, Rodovia Bambuí/Medeiros, Km-05, 38900-000 Bambuí, Minas Gerais, Brazil
[9]Departamento de Ecologia, Universidade Estadual Paulista, 13506-900 Rio Claro, São Paulo, Brazil

(iD) KW, 0000-0002-9550-4249; EB, 0000-0001-8157-8792

Wildfires produce substantial $CO_2$ emissions in the humid tropics during El Niño-mediated extreme droughts, and these emissions are expected to increase in coming decades. Immediate carbon emissions from uncontrolled wildfires in human-modified tropical forests can be considerable owing to high necromass fuel loads. Yet, data on necromass combustion during wildfires are severely lacking. Here, we evaluated necromass carbon stocks before and after the 2015–2016 El Niño in Amazonian forests distributed along a gradient of prior human disturbance. We then used Landsat-derived burn scars to extrapolate regional immediate wildfire $CO_2$ emissions during the 2015–2016 El Niño. Before the El Niño, necromass stocks varied significantly with respect to prior disturbance and were largest in undisturbed primary forests ($30.2 \pm 2.1$ Mg ha$^{-1}$, mean $\pm$ s.e.) and smallest in secondary forests ($15.6 \pm 3.0$ Mg ha$^{-1}$). However, neither prior disturbance nor our proxy of fire intensity (median char height) explained necromass losses due to wildfires. In our 6.5 million hectare (6.5 Mha) study region, almost 1 Mha of primary (disturbed and undisturbed) and 20 000 ha of secondary forest burned during the 2015–2016 El Niño. Covering less than 0.2% of Brazilian Amazonia, these wildfires resulted in expected immediate $CO_2$ emissions of approximately 30 Tg, three to four times greater than comparable estimates from global fire emissions databases. Uncontrolled understorey wildfires in humid tropical forests during extreme droughts are a large and poorly quantified source of $CO_2$ emissions.

This article is part of a discussion meeting issue 'The impact of the 2015/2016 El Niño on the terrestrial tropical carbon cycle: patterns, mechanisms and implications'.

## 1. Introduction

Increased concentrations of atmospheric $CO_2$ during El Niño Southern Oscillation events [1,2] have largely been attributed to emissions from the tropics [3,4], with wildfires playing an important role [4,5]. In recent decades, despite a global

**Table 1.** Forest classifications for pre-El Niño forest disturbance classes and the plot samples in 2010, 2014–2015 and 2017. The 2015–2016 sample occurred after extensive wildfires and is a subset of the 2014–2015 sample.

| pre-El Niño forest class | definition | necromass assessment (2010) | monitoring of CWD (2014–2015) | burned in 2015–2016 and sampled in 2017 | additionally burned area sampling (2017) |
| --- | --- | --- | --- | --- | --- |
| undisturbed primary forest | primary forest with no evidence of human disturbance, such as fire scars or logging stumps | 17 | 5 | 2 | 3 |
| logged primary forest | primary forest with evidence of logging, such as logging stumps | 26 | 5 | 4 | 1 |
| burned primary forest | primary forest with evidence of recent fire, such as fire scars | 7 | 0 | 0 | 0 |
| logged-and-burned primary forest | primary forest with evidence of both logging and fire | 24 | 4 | 1 | 4 |
| secondary forest | forest regenerating after complete removal of native vegetation | 33 | 4 | 0 | 1 |

reduction in burned vegetation area [6,7], relatively low-intensity understorey wildfires that spread from agricultural lands have increased in the fire-sensitive Amazon rainforest [8–11]. $CO_2$ emissions from such wildfires are expected to grow further [10] as fire-conducive weather patterns increase across the humid tropics, particularly in South America [12].

Large-scale understorey wildfires in Amazonia are unprecedented in recent millennia. During pre-Columbian times, fires were limited to those occurring naturally from lightning strikes and prescribed burns by indigenous peoples [13]. These fires were localized and prescribed burns were planned in accordance with environmental and ecological conditions [13]. However, pervasive human modification of tropical forest landscapes, through, for example, road building, cattle ranching and timber exploitation, combined with severe drought events and the widespread use of fire as a land management tool, has fundamentally altered Amazonian fire regimes. Today, uncontrolled large-scale understorey wildfires are being witnessed in the Amazon with sub-decadal frequency [14]. Such wildfires result in high rates of tree mortality [15,16], shifts in forest structure [17,18] and drier microclimatic conditions [19], ultimately leading to increased susceptibility to future wildfires [19–21].

Carbon emissions from understorey wildfires can be split into committed and immediate emissions. Committed emissions result from the complex interplay between delayed tree mortality and decomposition, and are dependent on future climatic conditions and human influences. Research indicates that long-term storage of carbon in wildfire-affected Amazonian forests can be compromised for decades: even 31 years after a fire event, burned forests store approximately 25% less carbon than unburned control sites owing to high levels of tree mortality that are not compensated by regrowth [22]. Immediate understorey emissions are those that occur during wildfires and, in contrast to committed emissions, are relatively simple to estimate. Biome- and continent-wide analyses that rely on satellite observations (known as top-down studies) suggest that these immediate emissions from tropical forests can be substantial [23,24] and, for example, can transform the

Amazon basin from a carbon sink to a large carbon source during drought years [25].

One potentially important source of immediate carbon emissions during wildfires is dead organic matter found on forest floors. This necromass, which includes leaf litter and woody debris, is a fundamental component of forest structure and dynamics and can account for up to 40% of the carbon stored in humid tropical forests [26–28]. During long periods of drought, this large carbon pool can become highly flammable [29]. However, studies quantifying necromass stocks have overwhelmingly focused on undisturbed primary forests [27]; studies that estimate necromass in human-modified tropical forests—forests that have been structurally altered by anthropogenic disturbance, such as selective logging and fires, and those regenerating following deforestation (commonly called *secondary forests*; table 1)—are rare (cf. [30,31]). This represents a key gap in our understanding because human-modified tropical forests are increasingly prevalent [32] and increasingly vulnerable to wildfires [33–35]. While many local-scale, bottom-up studies have quantified combustion characteristics and carbon emissions following fires related to deforestation and slash-and-burn practices (see Van Leeuwen *et al.* [36] for a recent review), we know of no study that quantifies necromass before and after uncontrolled understorey wildfires in human-modified Amazonian forests. These knowledge gaps and data shortfalls limit our understanding of immediate carbon emissions from understorey wildfires. Improving such estimates is essential for refining Earth Systems models and both national and global estimates of greenhouse gas emissions.

Here, we address these knowledge gaps using a hybrid bottom-up/top-down approach to study a human-modified region of central-eastern Amazonia that experienced almost 1 million hectares (1 Mha) of understorey wildfires during the 2015–2016 El Niño (figure 1). We combine data from a previously published large-scale field assessment of carbon stocks [37] with on-the-ground measures of woody debris before and after the 2015–2016 El Niño, proxies of fire intensity and coverage within study plots, and remotely sensed analyses of fire extent across the region. Specifically, we (a) quantify carbon
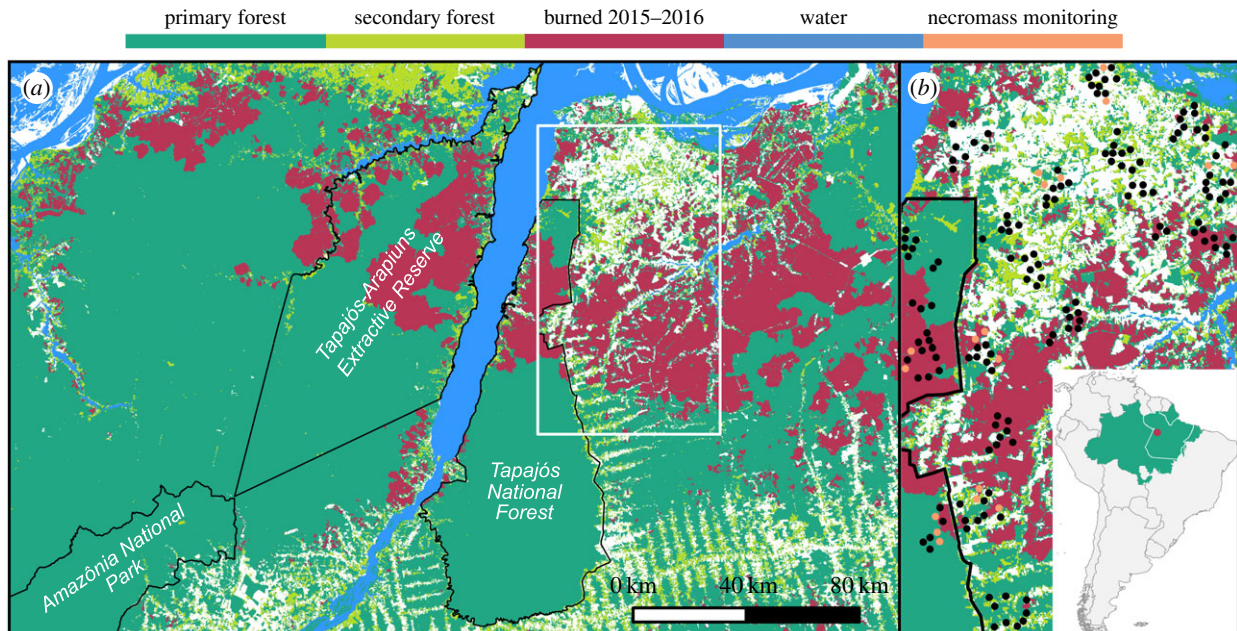
**Figure 1.** (a) The 2017 land-use map across the approximately 6.5 Mha study region. (b) The land-use map within the RAS study area (shown by the white border in (a)). Also shown in this panel are the locations of the 107 study plots (black circles). The 18 of these that were used for necromass monitoring are shown as orange circles. The inset shows the Santarém study region (red circle) within South America, the Brazilian Amazon (green) and Pará (white border).

stocks vulnerable to combustion across human-modified tropical forests in central-eastern Amazonia, (b) use post-burn measures to investigate the factors influencing the loss of necromass during wildfires, (c) estimate region-wide immediate carbon emissions from wildfires and (d) compare these region-wide emission estimates with those derived from widely used global fire emissions databases.

## 2. Methods

### (a) Quantifying necromass stocks in human-modified Amazonian forests

We established 107 plots (0.25 ha) in human-modified forests in central-eastern Amazonia in 2010 (figure 1). Plots were located in the municipalities of Santarém, Belterra and Mojuí dos Campos in the state of Pará, Brazil, and form part of the Sustainable Amazon Network (*Rede Amazônia Sustentável* (RAS) in Portuguese [38]). Study plots covered a range of prior human impacts (table 1) and included undisturbed primary forests ($n = 17$), primary forests selectively logged prior to 2010 ($n = 26$), primary forests burned prior to 2010 ($n = 7$), primary forests logged and burned prior to 2010 ($n = 24$) and secondary forests recovering after complete removal of vegetation ($n = 33$; table 1).

Summary carbon estimates for these 107 plots can be found in Berenguer *et al.* [37]. Here, we focused on carbon stored in their necromass pools. We estimated necromass stocks in dead-standing tree and palm stems, coarse woody debris (CWD; $\geq 10$ cm diameter at one extremity), fine woody debris (FWD; $\geq 2$ and $<10$ cm diameter at both extremities) and leaf litter (including twigs $<2$ cm diameter at both extremities, leaves, and fruits and seeds). Full carbon estimation methods can be found in Berenguer *et al.* [37]. In brief, in each plot, we measured the diameter and height of all large (greater than or equal to 10 cm diameter at breast height (DBH)) dead tree and palm stems. We measured the diameter and height of all small dead tree and palm stems ($\geq 2$ and $<10$ DBH) in five subplots ($5 \times 20$ m) in each plot. We used the allometric equations of Hughes *et al.* [39] and Cummings *et al.* [40] to estimate, respectively, carbon stocks for dead-standing trees and palms. Subplots were also

used to estimate the diameters and lengths of all pieces of fallen CWD. We estimated the volume of each piece of CWD using Smalian's formula [27] after accounting for the extent of damage (i.e. void space). We multiplied the volume of each CWD piece by its decomposition class to calculate CWD mass [30]. In all study plots, we established five smaller subplots ($2 \times 5$ m) to assess FWD. This was sampled and weighed in the field. A subsample ($\leq 1$ kg) was collected in each subplot and oven-dried to a constant weight. The wet-to-dry ratios of the FWD samples were used to estimate the total FWD stocks per plot. To estimate the biomass of leaf litter, ten $0.5 \times 0.5$ m quadrats were established in each plot. We oven-dried leaf litter samples to a constant weight to get an estimate of the leaf litter stocks in each plot. Biomass estimates for each necromass component were then standardized to per hectare values, and the carbon content was assumed to be 50% of biomass dry weight [41]. See electronic supplementary materials (§1) for all equations we used to estimate necromass biomass.

### (b) Longitudinal monitoring of coarse woody debris

To estimate necromass change through time, we continued to monitor 18 of the 107 RAS plots (figure 1). These 18 plots were chosen because they are spatially distributed across the region and we were able to secure long-term authorization to monitor them. They included undisturbed primary forests ($n = 5$), primary forests logged prior to 2010 ($n = 5$), primary forest logged and burned prior to 2010 ($n = 4$), and secondary forests ($n = 4$; table 1). We conducted surveys of the 18 plots between November 2014 and September 2015, using a slightly altered sampling design to align with the Global Ecosystem Monitoring protocol (see [42] for details). We established five $1 \times 20$ m subplots in each of the 18 plots, measured all pieces of CWD, and estimated their biomass and carbon content following the methods outlined above (see Methods (a)).

### (c) Impacts of El Niño-mediated wildfires on necromass stocks

Extensive understorey wildfires burned seven of our 18 study plots during the 2015–2016 El Niño, including two previously undisturbed primary forests, four primary forests logged prior to

2010, and one primary forest that was logged and burned prior to 2010. To investigate necromass carbon stock losses due to these wildfires, we resurveyed all 18 plots in June 2017. We re-measured each individual piece of CWD and estimated biomass using the methods described above (Methods (a)). By comparing CWD stocks before and after the El Niño in the 11 plots that did not experience wildfires, we were able to estimate CWD background decomposition rates. By comparing CWD stocks before and after the El Niño in the seven plots that burned, we were able to measure CWD combustion completeness.

We used values from the 2010 surveys to provide estimates of the pre-El Niño carbon stocks in leaf litter and FWD. Based on visual inspection of the sites (electronic supplementary material, figure S1), we assumed 100% combustion completeness of these necromass components in the fire-affected proportion of burned plots. Recognizing that this is a strong assumption, we consider the validity of it in our Discussion. We did not consider wildfire-mediated changes in necromass carbon stocks in dead-standing trees and palms, owing to a lack of data on combustion completeness.

In the seven plots that burned, we calculated average char height for each stem, defined as the sum of the maximum and minimum char heights divided by two. We then used these average stem char heights to calculate the plot-level median char height, which we used as our proxy for fire intensity. In addition, we used the proportion of sampled stems with burn scars as an estimate of the area of each plot that burned (electronic supplementary materials). To increase our sample of fire-affected plots (to 16), we also measured the area burned in an additional nine of the original RAS plots that were sampled during the 2010 censuses and burned during 2015–2016 (table 1). Prior to the wildfires, these additional plots included undisturbed primary forests ($n = 3$), primary forests logged prior to 2010 ($n = 1$), primary forests logged and burned prior to 2010 ($n = 4$), and secondary forests ($n = 1$).

We used these data to estimate the per hectare necromass loss (NL) attributable to wildfires using the following equation:

$$NL = FL_{CWD} \times (CC_{CWD} - D_{CWD}) + FL_{LLFWD} \times BA, \quad (2.1)$$

where $FL_{CWD}$ is the per hectare fuel load of CWD estimated from the 107 RAS plots surveyed in 2010, $CC_{CWD}$ is the combustion completeness of CWD estimated from seven of the 18 CWD monitoring plots that burned during the 2015–2016 El Niño, $D_{CWD}$ is the background CWD decomposition rate estimated from the 11 CWD monitoring plots that did not burn during the 2015–2016 El Niño, $FL_{LLFWD}$ is the per hectare fuel load of leaf litter and FWD estimated from the 107 plots surveyed in 2010, and BA is the proportion of the plot that burned estimated from the 16 RAS plots that burned (seven necromass monitoring sites and nine additional sites in which burned area was estimated) during the 2015–2016 El Niño (table 1).

## (d) Data analysis

We used the Kruskal–Wallis test to investigate variation across forest classes of prior human disturbance (table 1) and used the Conover–Iman test with Bonferroni adjustments to perform multiple pairwise comparisons of forest class medians. We assessed differences across forest classes in: carbon stocks stored in each necromass component (i.e. dead-standing stems, CWD, FWD and leaf litter) from the 2010 survey; total and percentage necromass carbon stock losses in the 18 plots surveyed between 2014 and 2017; and the proportion/area of plots burned during the 2015–2016 El Niño. We used linear regression to investigate the relationship between: necromass carbon stocks before and after the 2015–2016 El Niño; fire intensity and stock losses; and the burned area in each plot and stock losses.

## (e) Estimating burned area and region-wide emissions from forest fires

To estimate wildfire-mediated carbon emissions from necromass across our study region, we first calculated the cumulative area of primary and secondary forest that experienced understorey wildfires during 2015–2016 in the central-eastern region of the Amazon, an area of approximately 6.5 Mha (figure 1). We built a time-series of Landsat (5, 7 and 8) imagery from 2010 to 2017 for the RAS study region and the surrounding area from the EROS Science Processing Architecture (ESPA)/U.S. Geological Survey (USGS) website (https://espa.cr.usgs.gov). We performed an unsupervised classification of raw imagery, followed by manual correction of classification errors, to identify several land-uses throughout the time-series (see electronic supplementary material, table S2 for all land-use classes and §2 for a detailed description of burned area detection). We then used the burned area of primary and secondary forests and estimates of per hectare necromass stock losses from wildfires (equation (2.1)) to determine region-wide necromass carbon emissions, using a conversion factor of 3.286 kg of $CO_2$ per kg of C [43]. This conversion factor does not include other forms of emitted C (such as CO), in keeping with global fire emissions databases.

We took two approaches to account for uncertainty in expected regional necromass emissions. First, we considered four land-use scenarios using two sets of primary and secondary forests (electronic supplementary material, table S1). To account for potential variation in fire susceptibility across primary forest disturbance classes, we estimated the five variables in equation (2.1) using all undisturbed and disturbed primary forest classes (prim1) and then only disturbed primary forests (prim2). For secondary forests, we used $CC_{CWD}$ and $FL_{LLFWD}$ from all secondary forests, used $D_{CWD}$ and BA from all forest classes combined, and used $CC_{CWD}$ from all primary forest classes because none of the secondary forest plots we were monitoring for changes in CWD burned during 2015–2016 (sec1). Our other scenario for secondary forests (sec2) was more restrictive: we used the fuel load ($FL_{CWD}$, $FL_{LLFWD}$), decomposition ($D_{CWD}$), and BA values from secondary forests only and combined these with all $CC_{CWD}$ values we had from disturbed and undisturbed primary forests.

Second, to account for uncertainty in the distribution of the variables in equation (2.1), we ran 1000 bootstrap with replacement simulations to determine each variable's mean value and standard error. We calculated the standard error of equation (2.1) using the variable standard errors, accounting for error propagation, and we constructed 95% confidence intervals for equation (2.1) as its mean value $\pm$ 1.96 times the standard error of the mean.

## (f) Emissions and burned area comparisons with global databases

We compared our region-wide $CO_2$ emission estimates with two fire emissions databases frequently used in Earth Systems models and carbon budgets: the Global Fire Emissions Database (GFED) version 4.1s [44] and the Global Fire Assimilation System (GFAS) version 1.1 [45]. For both datasets, we obtained data for our study period (August 2015–July 2016) and cropped them to our approximately 6.5 Mha study region, shown in figure 1.

We first calculated cumulative emissions from GFED and GFAS (electronic supplementary material) and compared these with our emissions estimates. Second, to investigate potential sources of discrepancy between estimates, we spatially mapped GFED, GFAS and our $CO_2$ emissions estimates. At both GFED and GFAS resolutions (0.25° and 0.1°, respectively), we mapped our mean (across land-use scenarios; electronic supplementary material, table S1) expected emissions assuming that emissions were constant in a burned area (i.e. if a cell contained $x$% of the burned area, we assumed it accounted for $x$% of the total emissions). Finally, because
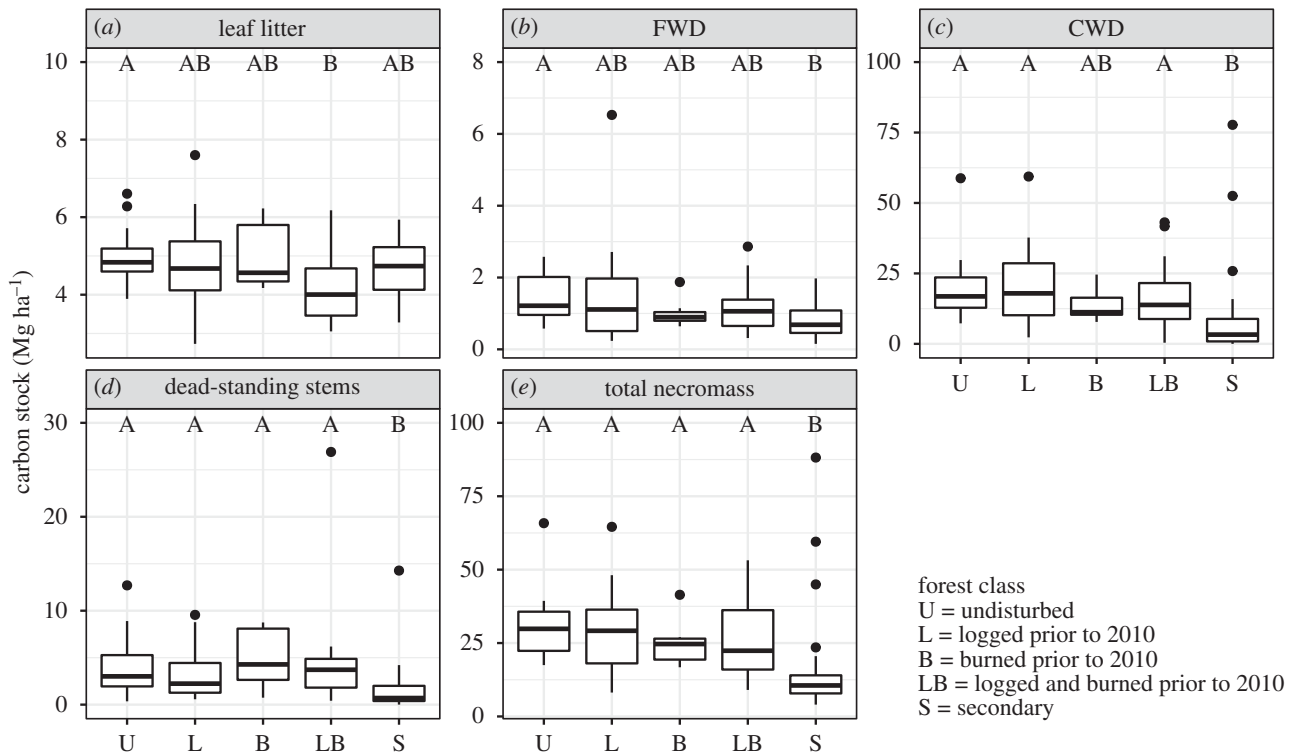
**Figure 2.** Necromass carbon stocks in leaf litter (*a*), FWD (*b*), CWD (*c*) and dead standing stems (*d*), and the total across all components (*e*) in human-modified Amazonian forests. Boxplots show the interquartile range. Letters above the boxplots show the results from multiple pairwise comparisons of forest class medians. Classes that do not share a letter have significantly different medians ( $p < 0.05$ ).

GFED also provides estimates of the area burned at 0.25°, we used our land-use map to estimate burned area at that resolution.

## 3. Results

### (a) Necromass carbon stocks across human-modified Amazonian forests

Total necromass and its components varied significantly with respect to forest class ( $p < 0.05$ in all cases; figure 2). Primary forests contained significantly higher total necromass than secondary forests ( $p < 0.01$ for all pairwise comparisons), with the highest total found in undisturbed primary forests (30.2 ± 2.1 Mg ha$^{-1}$, mean ± s.e.). By contrast, secondary forests contained only half as much necromass as undisturbed primary forests (15.6 ± 3.0 Mg ha$^{-1}$). Variation in total necromass was driven in large part by variation in CWD, which accounted for 61.3 ± 2.7% of the total necromass stocks across forest classes. Leaf litter was the next most important component of total necromass, with 19.8 ± 2.7% residing in this component. Dead-standing stems accounted for 14.4 ± 1.8% of total necromass. Finally, FWD was by far the smallest necromass component, harbouring just 4.6 ± 0.2% of the total.

### (b) Impacts of El Niño-mediated wildfires on necromass stocks

On average, we estimate that 87.1 ± 2.7% of the ground area of our fire-affected study plots burned, and there was no significant difference in the total burned area of fire-affected plots across forest classes ( $\chi_3^2 = 2.1$ ; $p = 0.56$ ). From the 88 CWD pieces measured before the fires, 54 completely burned, 32 had partial combustion, and two were untouched by fire. CWD carbon stock losses from combustion varied from 38 to 94% (mean 65.4%, s.e. 7.1%) at the plot-level.

Necromass carbon stock losses in the seven burned plots were unrelated to median char height ( $R^2 = 0.09$ ; $p = 0.51$ ; figure 3*a*) and area of plot burned ( $R^2 = 0.10$ ; $p = 0.49$ ; figure 3*b*). Forest class did not predict necromass carbon stock losses in burned sites when expressed as either percentage ( $\chi_2^2 = 2.25$ ; $p = 0.32$ ) or total ( $\chi_2^2 = 1.12$ ; $p = 0.57$ ) loss. Similarly, forest class did not predict necromass losses in unburned sites when expressed as either percentage ( $\chi_3^2 = 1.58$ ; $p = 0.66$ ) or total ( $\chi_3^2 = 2.18$ ; $p = 0.54$ ) loss.

On average, burned sites lost 73.0 ± 4.9% of their pre-El Niño necromass stocks (figure 4), compared with a 26.1 ± 4.8% reduction in unburned sites (from decomposition). As expected, pre-El Niño necromass stocks strongly predicted post-El Niño necromass in our unburned sites ( $R^2 = 0.95$ ; $p < 0.001$ ; figure 4*a*). This relationship disappeared in fire-affected plots ( $R^2 = 0.08$ ; $p = 0.54$ ; figure 4*b*), indicating that combustion completeness was insensitive to initial necromass stocks. Despite our small sample size, visual inspection suggests that these findings were unaffected by forest class.

### (c) Region-wide burned area and estimates of carbon stock losses

During the 2015–2016 El Niño, 15.2% of our study region and 982 276 ha of forest experienced understorey wildfires. These wildfires were overwhelmingly concentrated in primary forests: less than 2% of the burned area was in secondary forests, despite these accounting for 9% of the forest cover in our study region. When considering all primary and secondary forest plots (prim1 + sec1), resultant necromass carbon stock losses amounted to 10.06 Tg (95% confidence interval, 5.85–14.27 Tg). Converting to $CO_2$, this is equivalent to expected emissions of 33.05 Tg (95% confidence interval, 19.22–46.87 Tg; figure 5). Our mean $CO_2$ emission estimates were relatively insensitive to the
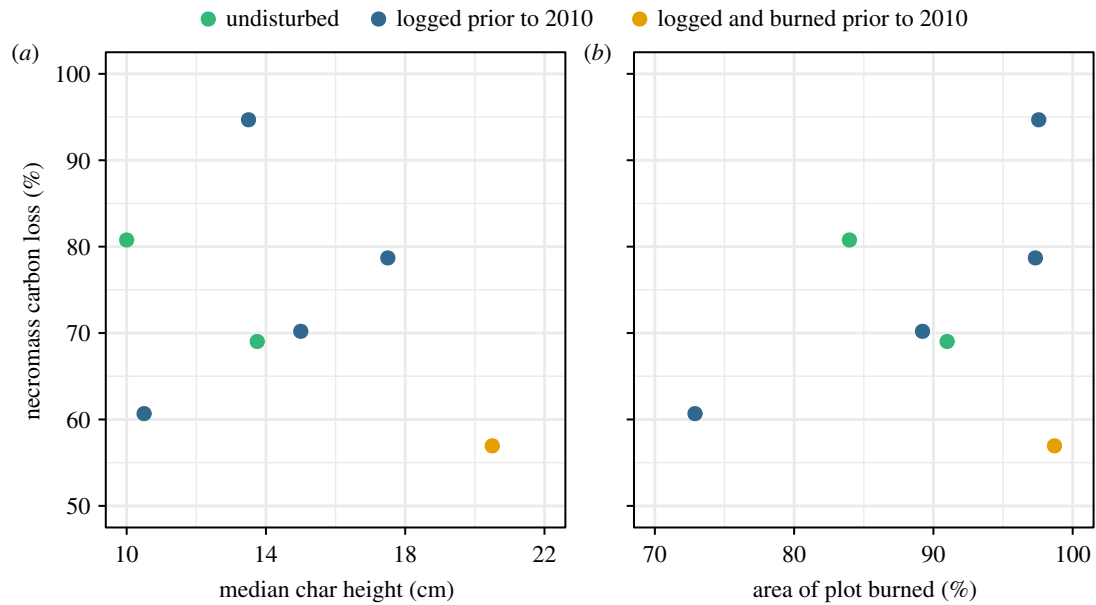
**Figure 3.** (*a*) Necromass carbon stock losses and fire intensity, as measured by median char height. (*b*) Necromass carbon stock losses and area of plot burned.
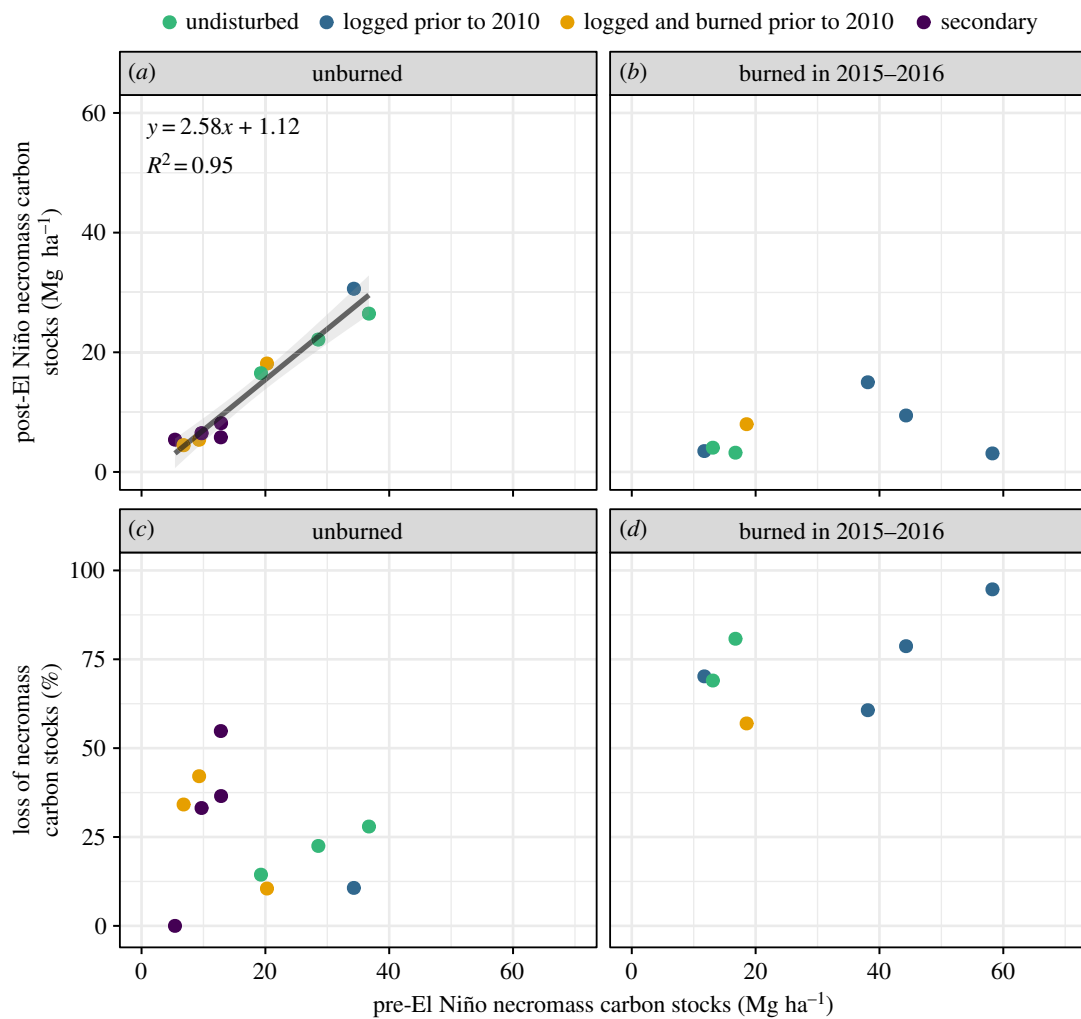


**Figure 4.** Pre- versus post-El Niño necromass carbon stocks in unburned control sites (*a*) and sites burned in 2015–2016 (*b*), and pre-El Niño necromass carbon stocks versus post-El Niño necromass losses in unburned control sites (*c*) and sites burned in 2015–2016 (*d*) in human-modified Amazonian forests. In panel (*a*) the black line shows the significant ($p < 0.001$) relationship between pre- and post-El Niño necromass carbon stocks in unburned sites. The equation for this relationship is shown in the panel. The grey band represents 1 s.e.m. Note that, owing to data limitations, pre- and post-El Niño necromass totals are based on CWD, FWD and leaf litter only (i.e. dead-standing stems are not included).
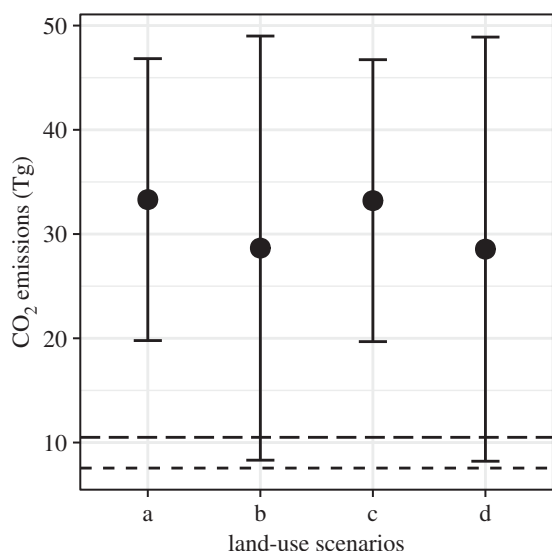
**Figure 5.** Immediate $CO_2$ emissions for wildfires in central-eastern Amazonian human-modified tropical forests. Points show expected emissions for four land-use scenarios (see §2e and electronic supplementary material, table S1): (a) prim1 + sec1; (b) prim2 + sec1; (c) prim1 + sec2; (d) prim2 + sec2. Error bars show 95% confidence intervals. Also shown are cumulative $CO_2$ emissions for our study region and period from GFED 4.1s (short-dashed line) and GFAS version 1.1 (long-dashed line).

land-use scenarios (figure 5). However, the 95% confidence interval was substantially wider with land-use scenario prim2 (scenarios b and d; figure 5) owing to greater uncertainty in decomposition rates when restricted to disturbed primary forest only compared with all primary forests—undisturbed and disturbed—combined.

## (d) Comparing our results with global fire emission databases

Both GFED and GFAS vastly underestimated expected wildfire $CO_2$ emissions for our study region and period. Respectively, these databases suggest cumulative emissions that are 77% and 68% lower than the expected value we found with land-use scenario a (prim1 + sec1; figure 5). These discrepancies can be explained by the underdetection of understorey wildfires by both GFED and GFAS algorithms. This can be seen across our whole study region but is particularly evident in areas free from historic deforestation (figure 6). GFED and GFAS appeared to be more successful at detecting fires in agricultural areas with lower levels of forest cover (figure 6). Highlighting the insensitivity of GFED to understory wildfires, this database suggests that, at most, 6% of any given 0.25° cell across our study region, and approximately 90 000 ha in total, burned during the 2015–2016 El Niño (figure 6e). By contrast, we show that as much as 74% of a cell (figure 6f) and almost 1 Mha of forest was affected by understory wildfires.

## 4. Discussion

### (a) Region-wide carbon emissions from El Niño-mediated wildfires

We investigated necromass carbon stocks in human-modified forests before and after large-scale understorey wildfires in central-eastern Amazonia that occurred during the 2015–2016 El Niño. Our novel assessment revealed that expected immediate

necromass $CO_2$ emissions from these wildfires are around 30 Tg (figure 5). This is equivalent to total $CO_2$ emissions from fossil fuel combustion and the production of cement in Denmark, or 6% of such emissions from Brazil, in 2014 [46]. Consequently, wildfire-mediated immediate carbon emissions, which are not currently considered under national greenhouse gas inventories [47], represent a large source of $CO_2$ emissions. Moreover, these immediate emissions will be greatly exacerbated by further committed emissions resulting from tree mortality, which can be as high as 50% [16] and may not be balanced by post-fire regrowth on decadal time scales [22].

Our results add to work on prescribed burns associated with deforestation [36], contributing important information about the role of El Niño-mediated wildfires. The scale of the immediate emissions we estimated, coupled with future committed emissions, make wildfires particularly relevant to climate change mitigation programmes such as REDD+ [9,48]. For REDD+ to succeed in Amazonia, we demonstrate that forests must be protected from wildfires, as even the immediate emissions from large-scale wildfires can equal those from whole countries. Future climate change will make this only more imperative, with extreme droughts, higher temperatures, and reduced rainfall all predicted for the Amazon basin in the near future [49–51]. Wildfires may also undermine the important role that protected areas have historically served as carbon stores [52], as illustrated by the large areas burned in the Tapajós National Forest and the Tapajós-Arapiuns Extractive Reserve (figure 1).

### (b) Fuel loads in humid tropical forests

Total necromass carbon stocks in the 107 RAS plots surveyed in 2010 did not vary significantly between disturbed and undisturbed primary forests (figure 2e). The mean value we found for total necromass carbon stocks in undisturbed forests was $30.2 \pm 2.1$ Mg ha$^{-1}$. This value is broadly consistent with previous estimates for the eastern Amazon. For example, Keller et al. [30] and Palace et al. [31] found necromass carbon stocks of, respectively, 25.4 and 29.2 Mg ha$^{-1}$ in undisturbed primary forests in the Tapajós region of Pará. In primary forests disturbed by reduced-impact logging, these studies found, respectively, 36.4 and 42.75 Mg ha$^{-1}$ of necromass carbon. However, our estimates for necromass stocks in disturbed primary forests are markedly lower (figure 2e). This discrepancy is likely a function of time since disturbance. Keller et al. [30] and Palace et al. [31] assessed necromass carbon stocks soon after disturbance, when necromass stocks are likely to be higher. By contrast, disturbance of RAS sites occurred between 1.5 and 25 years before the 2010 surveys. Necromass stocks can be highly dynamic, with residence times for most CWD estimated at less than a decade [28], especially in the case of small diameter and low wood density tree species [53]. Thus, necromass stocks in many of our disturbed primary forest sites may have had time to decrease to an equilibrium level, similar to that of undisturbed forests, where input and decomposition are largely balanced.

We did, however, find significantly larger necromass stocks in primary forests compared with secondary forests. This may be explained by (a) pre-abandonment secondary forest land-uses removing all fallen biomass with machinery or intensive fires; (b) the smaller necromass input pool in secondary forests owing to lower levels of aboveground live biomass [37]; and
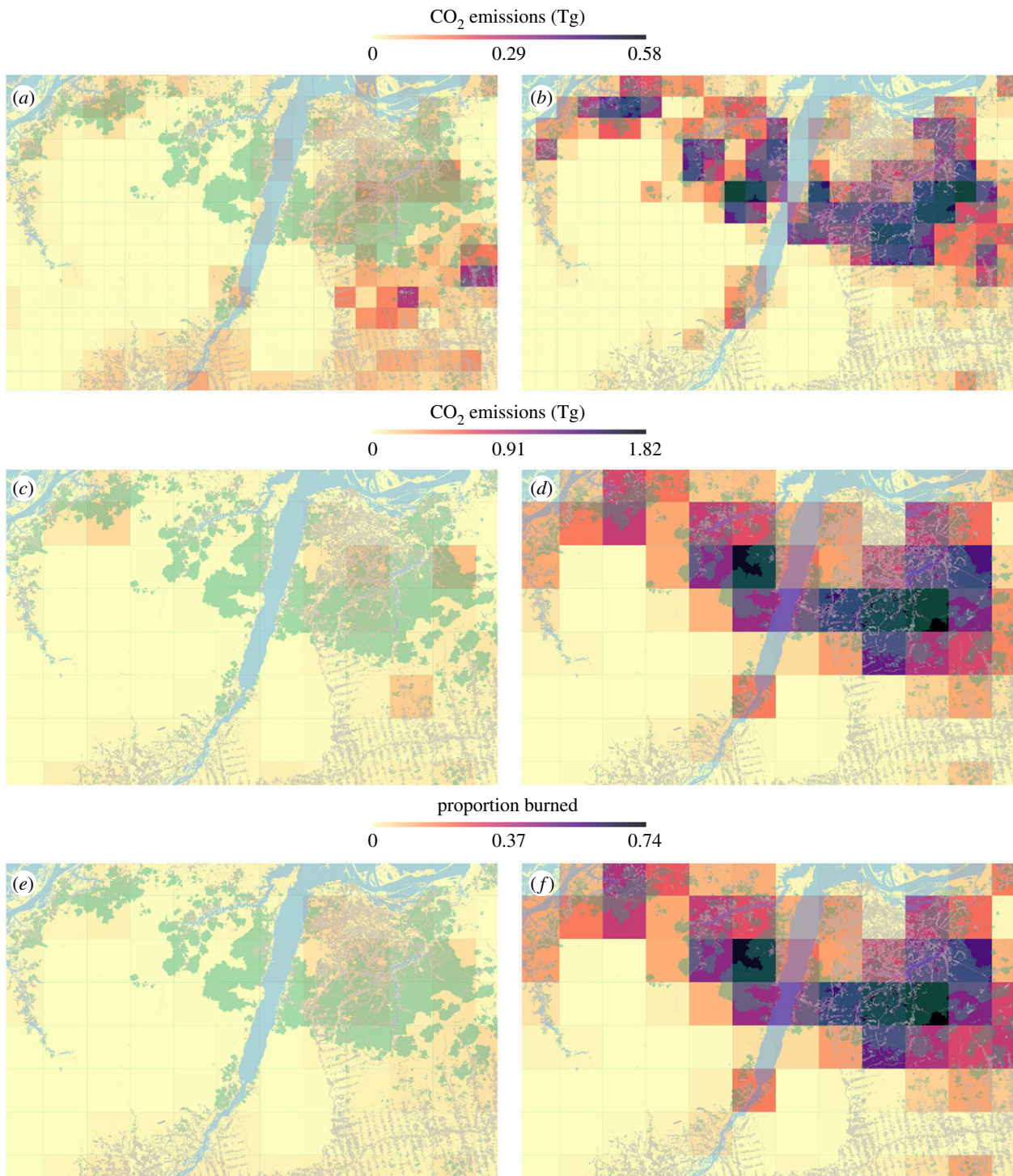
**Figure 6.** Comparing our findings with those from GFAS and GFED. $CO_2$ emissions for our study region and period from GFAS (*a*) and our emissions shown at the same scale (0.1°; (*b*)). $CO_2$ emissions from GFED (*c*) and our emissions shown at the same scale (0.25°; (*d*)). The proportion of land burned for our study region and period from GFED (*e*) and our estimate of burned area shown at the same scale (0.25°; (*f*)). In all panels, our Landsat-derived fire map is shown in dark green, deforestation in light grey and water in blue.

(c) the lower wood density of stems in secondary forests [54], resulting in more rapid CWD decomposition.

## (c) Impacts of El Niño-mediated wildfires on necromass stocks

On average, we estimate that wildfires burned $87.1 \pm 2.7\%$ of our fire-affected necromass monitoring plots (figure 3*b*). This figure is substantially higher than the 62–75% burn coverage measured during experimental fires in previously undisturbed transitional Amazonian forests [18]. The areal extent of these

wildfires reduced necromass (in CWD, FWD and leaf litter) carbon stocks by $46.9 \pm 6.9\%$, when gross necromass loss ($73.0 \pm 4.9\%$) was corrected for decomposition ($26.1 \pm 4.8\%$). The understorey wildfires that affected our burned plots were relatively low intensity, with maximum median char height of 20.5 cm. Nonetheless, our findings demonstrate that these low-intensity wildfires can dramatically diminish necromass stocks in human-modified tropical forests.

Further, both area of plot burned and necromass carbon stock losses showed little variation across disturbance classes. This may indicate that the 2015–2016 El Niño, which was

one of the strongest in recorded history, produced drought conditions so severe that necromass moisture content was reduced across all forest classes to a level that permitted combustion and sustained fires, overriding any pre-existing microclimatic differences that may have existed owing to the initial disturbance. This is further corroborated by the fact that wildfires did not distinguish between largely undisturbed forests (mostly inside protected areas) and those that have been modified by humans (mostly outside protected areas), burning vast areas of both types of forest (figure 1).

## (d) Caveats

Though our dataset is the first to our knowledge that allows for quantification of necromass carbon stocks pre- and post-uncontrolled understorey wildfires in human-modified Amazonian forests, our sample size was limited, with just 18 necromass monitoring plots, of which seven burned during the 2015–2016 El Niño. Consequently, results that follow from these samples should be treated with a degree of caution. In particular, we found that necromass stock losses were not significantly related to our plot-level estimate of burned area and that fire susceptibility did not appear to vary across disturbance classes. In both cases, the lack of significance may reflect the small sample sizes rather than a genuine lack of relationship.

Moreover, owing to the limitations of our data, we assumed 100% combustion of leaf litter and FWD in the fraction of plots that burned when calculating necromass carbon losses (equation (2.1)). In a recent review, Van Leeuwen *et al*. [36] found that mean combustion completeness of leaves, litter and smaller classes of woody debris was 73–94%. However, as they acknowledge, combustion completeness can be significantly higher during El Niño years. Thus, given the strength of the 2015–2016 El Niño, and our personal observations (electronic supplementary material, figure S1), our combustion completeness assumption is likely to be reasonable.

Because of our small sample size, the 95% confidence intervals for our region-wide $CO_2$ immediate emissions were wide, ranging from around 8 Tg to almost 48 Tg. Future research efforts should prioritize necromass monitoring in a larger number of sites, across a range of tropical forests, to better constrain these values; as we show, such emissions have the potential to significantly exacerbate global climate change.

Despite the above limitations, there are reasons to suspect that our necromass stock loss and carbon emission estimates are highly conservative. First, we did not measure wildfire-induced carbon changes in the soil organic layer, yet research from the same region suggests that wildfires significantly reduce soil carbon pools [55]; nor could we estimate combustion of dead-standing stems, which accounted for approximately 15% of total necromass (figure 2). Second, none of the disturbed primary forest plots in which we monitored necromass changes was recently disturbed prior to the 2015–2016 wildfires, allowing time for decomposition to reduce high levels of post-disturbance necromass. Had our sample included recently disturbed sites, necromass losses would have been greater. Third, detection of low-intensity understorey wildfires continues to present a remote sensing challenge. Although manual correction of our unsupervised land-use classifications revealed only a small number of misclassifications, it is possible that some wildfire-affected sites were missed, leading to an underestimation of regional emissions.

In addition to showing that wildfire carbon emissions can be substantial, we also showed that such emissions remain poorly quantified. GFED and GFAS, $CO_2$ emission databases that are widely used in Earth Systems models and carbon budgets, returned considerably lower emission estimates for our study region and period than our expected values (figure 5). Nevertheless, the scale of this discrepancy is underestimated for several reasons. First, we focused solely on necromass carbon losses from understory wildfires, whereas GFED and GFAS include emissions from all land-use classes combined. Both databases therefore account for grassland and agricultural fires, which can affect large areas of human-modified tropical landscapes. Second, GFED includes both committed and immediate $CO_2$ emissions. Third, and again with respect to GFED, fuel loads are much high than those present in our post-disturbance plots, because they are primarily derived from slash-and-burn and deforestation studies.

## (e) Conclusion

We demonstrate that there was a substantial loss of necromass following El Niño-mediated wildfires in the central-eastern Amazon. We conservatively estimate that wildfires in this region burned 982 276 ha (15.2% of our study region) of primary and secondary forest, resulting in expected immediate $CO_2$ emissions of approximately 30 Tg. Better understanding this large and poorly quantified source of atmospheric carbon is crucial for climate change mitigation efforts.

# References

1. Wang W *et al.* 2013 Variations in atmospheric $CO_2$ growth rates coupled with tropical temperature. *Proc. Natl Acad. Sci. USA* **110**, 13 061–13 066. (doi:10.1073/pnas.1219683110)

2. Betts RA, Jones CD, Knight JR, Keeling RF, Kennedy JJ. 2016 El Niño and a record $CO_2$ rise. *Nat. Clim. Change* **6**, 806–810. (doi:10.1038/nclimate3063)

3. Zeng N, Qian H, Roedenbeck C, Heimann M. 2005 Impact of 1998–2002 midlatitude drought and warming on terrestrial ecosystem and the global carbon cycle. *Geophys. Res. Lett.* **32**. (doi:10.1029/2005GL024607)

4. Wang J, Zeng N, Wang M, Jiang F, Wang H, Jiang Z. 2018 Contrasting terrestrial carbon cycle responses to the 1997/98 and 2015/16 extreme El Niño events. *Earth Syst. Dyn.* **95194**, 1–14. (doi:10.5194/esd-9-1-2018)

5. Fanin T, Van Der Werf GR. 2015 Relationships between burned area, forest cover loss, and land cover change in the Brazilian Amazon based on satellite data. *Biogeosciences* **12**, 6033–6043. (doi:10.5194/bg-12-6033-2015)

6. Andela N *et al.* 2017 A human-driven decline in global burned area. *Science* **356**, 1356–1362. (doi:10.1126/science.aal4108)

7. Arora VK, Melton JR. 2018 Reduction in global area burned and wildfire emissions since 1930s enhances carbon uptake by land. *Nat. Commun.* **9**, 1326. (doi:10.1038/s41467-018-03838-0)

8. Hardesty J, Myers R, Fulks W. 2005 Fire, ecosystems, and people: a preliminary assessment of fire as a global conservation issue. *George Wright Forum* **22**, 78–87. (doi:10.2307/43597968)

9. Aragão LEOC, Shimabukuro YE. 2010 The incidence of fire in Amazonian forests with implications for REDD. *Science* **328**, 1275–1278. (doi:10.1126/science.1186925)

10. Aragão LEOC *et al.* 2018 21st Century drought-related fires counteract the decline of Amazon deforestation carbon emissions. *Nat. Commun.* **9**, 536. (doi:10.1038/s41467-017-02771-y)

11. van Marle MJE, Field RD, van der Werf GR, Estrada de Wagt IA, Houghton RA, Rizzo LV, Artaxo P, Tsigaridis K. 2017 Fire and deforestation dynamics in Amazonia (1973–2014). *Global Biogeochem. Cycles* **31**, 24–38. (doi:10.1002/2016GB005445)

12. Jolly WM, Cochrane MA, Freeborn PH, Holden ZA, Brown TJ, Williamson GJ, Bowman DMJS. 2015 Climate-induced variations in global wildfire danger from 1979 to 2013. *Nat. Commun.* **6**, 7537. (doi:10.1038/ncomms8537)

13. Pivello VR. 2011 The use of fire in the Cerrado and Amazonian rainforests of Brazil: past and present. *Fire Ecol.* **7**, 24–39. (doi:10.4996/fireecology.0701024)

14. Chen Y, Randerson JT, Morton DC, DeFries RS, Collatz GJ, Kasibhatla PS, Giglio L, Jin Y, Marlier ME. 2011 Forecasting fire season severity in South America using sea surface temperature anomalies. *Science* **334**, 787–791. (doi:10.1126/science.1209472)

15. Brando PM *et al.* 2014 Abrupt increases in Amazonian tree mortality due to drought–fire interactions. *Proc. Natl Acad. Sci. USA* **111**, 6347–6352. (doi:10.1073/pnas.1305499111)

16. Barlow J, Peres CA, Lagan BO, Haugaasen T. 2003 Large tree mortality and the decline of forest biomass following Amazonian wildfires. *Ecol. Lett.* **6**, 6–8. (doi:10.1046/j.1461-0248.2003.00394.x)

17. Barlow J, Peres CA. 2004 Ecological responses to El Niño-induced surface fires in central Brazilian Amazonia: management implications for flammable tropical forests. *Phil. Trans. R. Soc. Lond. B* **359**, 367–380. (doi:10.1098/rstb.2003.1423)

18. Brando PM, Oliveria-Santos C, Rocha W, Cury R, Coe MT. 2016 Effects of experimental fuel additions on fire intensity and severity: unexpected carbon resilience of a neotropical forest. *Glob. Change Biol.* **22**, 2516–2525. (doi:10.1111/gcb.13172)

19. Cochrane MA, Schulze MD. 1999 Fire as a recurrent event in tropical forests of the eastern Amazon: effects on forest structure, biomass, and species composition. *Biotropica* **31**, 2–16. (doi:10.1111/j.1744-7429.1999.tb00112.x)

20. Alencar A, Asner GP, Knapp D, Zarin D. 2011 Temporal variability of forest fires in eastern Amazonia. *Ecol. Appl.* **21**, 2397–2412. (doi:10.1890/10-1168.1)

21. Cochrane MA, Alencar A, Schulze MD, Souza CM, Nepstad DC, Lefebvre P, Davidson EA. 1999 Positive feedbacks in the fire dynamic of closed canopy tropical forests. *Science* **284**, 1832–1835. (doi:10.1126/science.284.5421.1832)

22. Silva CVJ *et al.* 2018 Drought-induced Amazonian wildfires instigate a decadal-scale disruption of forest carbon dynamics. *Phil. Trans. R. Soc. B* **373**, 20180043. (doi:10.1098/rstb.2018.0043)

23. van der Laan-Luijkx IT *et al.* 2015 Response of the Amazon carbon balance to the 2010 drought derived with CarbonTracker South America. *Global Biogeochem. Cycles* **29**, 1092–1108. (doi:10.1002/2014GB005082)

24. Liu J *et al.* 2017 Contrasting carbon cycle responses of the tropical continents to the 2015–2016 El Niño. *Science* **358**, eaam5690. (doi:10.1126/science.aam5690)

25. Gatti LV *et al.* 2014 Drought sensitivity of Amazonian carbon balance revealed by atmospheric measurements. *Nature* **506**, 76–80. (doi:10.1038/nature12957)

26. Pan Y *et al.* 2011 A large and persistent carbon sink in the world's forests. *Science* **333**, 988–993. (doi:10.1126/science.1201609)

27. Chao K-J, Phillips OL, Baker TR, Peacock J, Lopez-Gonzalez G, Vásquez Martínez R, Monteagudo A, Torres-Lezama A. 2009 After trees die: quantities and determinants of necromass across Amazonia. *Biogeosciences* **6**, 1615–1626. (doi:10.5194/bg-6-1615-2009)

28. Palace M, Keller M, Hurtt G, Frolking S. 2012 A review of above ground necromass in tropical forests. In *Tropical forests* (ed. P Sudarshana), pp. 215–252. Rijeka, Croatia: InTech.

29. Ray D, Nepstad D, Moutinho P. 2005 Micrometeorological and canopy controls of fire susceptibility in a forested Amazon landscape. *Ecol. Appl.* **15**, 1664–1678. (doi:10.1890/05-0404)

30. Keller M, Palace M, Asner GP, Pereira R, Silva JNM. 2004 Coarse woody debris in undisturbed and logged forests in the eastern Brazilian Amazon. *Glob. Chang. Biol.* **10**, 784–795. (doi:10.1111/j.1529-8817.2003.00770.x)

31. Palace M, Keller M, Asner GP, Silva JNM, Passos C. 2007 Necromass in undisturbed and logged forests in the Brazilian Amazon. *For. Ecol. Manage.* **238**, 309–318. (doi:10.1016/j.foreco.2006.10.026)

32. Keenan RJ, Reams GA, Achard F, de Freitas JV, Grainger A, Lindquist E. 2015 Dynamics of global forest area: Results from the FAO Global Forest Resources Assessment 2015. *For. Ecol. Manage.* **352**, 9–20. (doi:10.1016/j.foreco.2015.06.014)

33. Cochrane MA. 2003 Fire science for rainforests. *Nature* **421**, 913–919. (doi:10.1038/nature01437)

34. Uhl C, Kauffman JB. 1990 Deforestation, fire susceptibility, and potential tree responses to fire in the eastern Amazon. *Ecology* **71**, 437–449. (doi:10.2307/1940299)

35. Alencar A, Nepstad D, Del Carmen Vera Diaz M. 2006 Forest understory fire in the Brazilian Amazon in ENSO and non-ENSO years: area burned and committed carbon emissions. *Earth Interact.* **10**, 1–7. (doi:10.1175/EI150.1)

36. Van Leeuwen TT *et al.* 2014 Biomass burning fuel consumption rates: a field measurement database. *Biogeosciences* **11**, 7305–7329. (doi:10.5194/bg-11-7305-2014)

37. Berenguer E *et al.* 2014 A large-scale field assessment of carbon stocks in human-modified tropical forests. *Glob. Change Biol.* **20**, 3713–3726. (doi:10.1111/gcb.12627)

38. Gardner TA *et al.* 2013 A social and ecological assessment of tropical land uses at multiple scales: the Sustainable Amazon Network. *Phil. Trans. R. Soc. B* **368**, 20120166. (doi:10.1098/rstb.2012.0166)

39. Hughes RF, Kauffman JB, Jaramillo VJ. 1999 Biomass, carbon, and nutrient dynamics of secondary forests in a humid tropical region of México. *Ecology* **80**, 1892–1907. (doi:10.1890/0012-9658(1999)080[1892:BCANDO]2.0.CO;2)

40. Cummings DL, Boone Kauffman J, Perry DA, Flint Hughes R. 2002 Aboveground biomass and structure of rainforests in the southwestern Brazilian Amazon. *For. Ecol. Manage.* **163**, 293–307. (doi:10.1016/S0378-1127(01)00587-4)

41. Eggleston HS, Intergovernmental Panel on Climate Change, National Greenhouse Gas Inventories Programme 2006 *2006 IPCC guidelines for national greenhouse gas inventories* (ed. C Kankyō, S Kenkyū, L Kikan, K Miwa). Kanagawa, Japan: Institute for Global Environmental Strategies.

See http://www.sidalc.net/cgi-bin/wxis.exe/
?IsisScript=earth.
xis&method=post&formato=2&cantidad=1
&expresion=mfn=001720.

42. Marthews TR *et al.* 2014 *Measuring tropical forest carbon allocation and cycling: a RAINFOR-GEM field manual for intensive census plots (v3.0)*. Global Ecosystems Monitoring Network. See http://gem.tropicalforests.ox.ac.uk/.

43. Akagi SK, Yokelson RJ, Wiedinmyer C, Alvarado MJ, Reid JS, Karl T, Crounse JD, Wennberg PO. 2011 Emission factors for open and domestic biomass burning for use in atmospheric models. *Atmos. Chem. Phys.* **11**, 4039–4072. (doi:10.5194/acp-11-4039-2011)

44. van der Werf GR *et al.* 2017 Global fire emissions estimates during 1997–2016. *Earth Syst. Sci. Data* **9**, 697–720. (doi:10.5194/essd-9-697-2017)

45. Kaiser JW *et al.* 2012 Biomass burning emissions estimated with a global fire assimilation system based on observed fire radiative power.

*Biogeosciences* **9**, 527–554. (doi:10.5194/bg-9-527-2012)

46. World Bank. 2018 CO$_2$ emissions. See https://data.worldbank.org/indicator/EN.ATM.CO2E.KT?view=chart (accessed 27 April 2018).

47. Bustamante MMC *et al.* 2016 Toward an integrated monitoring framework to assess the effects of tropical forest degradation and recovery on carbon stocks and biodiversity. *Glob. Change Biol.* **22**, 92–109. (doi:10.1111/gcb.13087)

48. Barlow J *et al.* 2012 The critical importance of considering fire in REDD+ programs. *Biol. Conserv.* **154**, 1–8. (doi:10.1016/J.BIOCON.2012.03.034)

49. Dai A. 2013 Increasing drought under global warming in observations and models. *Nat. Clim. Change* **3**, 52–58. (doi:10.1038/nclimate1633)

50. Malhi Y, Roberts JT, Betts RA, Killeen TJ, Li W, Nobre CA. 2008 Climate change, deforestation, and the fate of the Amazon. *Science* **319**, 169–172. (doi:10.1126/science.1146961)

51. Spracklen DV, Garcia-Carreras L. 2015 The impact of Amazonian deforestation on Amazon basin rainfall.

*Geophys. Res. Lett.* **42**, 9546–9552. (doi:10.1002/2015GL066063)

52. Soares-Filho B *et al.* 2010 Role of Brazilian Amazon protected areas in climate change mitigation. *Proc. Natl Acad. Sci. USA* **107**, 10 821–10 826. (doi:10.1073/pnas.0913048107)

53. Chambers JQ, Higuchi N, Schimel JP, Ferreira LV, Melack JM. 2000 Decomposition and carbon cycling of dead trees in tropical forests of the central Amazon. *Oecologia* **122**, 380–388. (doi:10.1007/s004420050044)

54. Berenguer E, Gardner TA, Ferreira J, Aragão LEOC, Mac Nally R, Thomson JR, Vieira ICG, Barlow J. In press. Seeing the woods through the saplings: using wood density to assess the recovery of human-modified Amazonian forests. *J. Ecol.* (doi:10.1111/1365-2745.12991)

55. Durigan MR *et al.* 2017 Soil organic matter responses to anthropogenic forest disturbance and land use change in the eastern Brazilian Amazon. *Sustainability* **9**, 379. (doi:10.3390/su9030379)